Dissociation dynamics of the water dication following one-photon double ionization. I. Theory

Zachary L. Streeter,[1,2] Frank L. Yip,[3] Robert R. Lucchese,[1] Benoit Gervais,[4]
Thomas N. Rescigno,[1] and C. William McCurdy[1,2,*]

[1]*Chemical Sciences Division, Lawrence Berkeley National Laboratory, Berkeley, California 94720, USA*
[2]*Department of Chemistry, University of California, Davis, California 95616, USA*
[3]*Department of Science and Mathematics, California State University-Maritime Academy, Vallejo, California 94590, USA*
[4]*CIMAP, Unité Mixte CEA-CNRS-ENSICAEN-UCBN 6252, BP 5133, F-14070 Caen, Cedex 05, France*

(Received 23 March 2018; published 26 November 2018)

The measurement of the triple differential cross section in the body frame for double photoionization of a molecule can be made in principle by detecting the ionic fragments and the two photoelectrons in coincidence—but only if the dynamics and geometry of dissociation of the doubly charged molecular ion are known. A classical trajectory study of the nine lowest states of the water dication is presented using high quality *ab initio* potential-energy surfaces. Sampling from a semiclassical initial distribution of positions and momenta is used to approximate ionization from the Frank-Condon region of the ground vibrational state of neutral H_2O. Excellent agreement in comparison with preliminary experimental momentum imaging measurements of double photoionization of water show that eight dication states can be unambiguously identified in the experiment with the aid of theory. The theoretical trajectory results allow body frame measurements of double photoionization to yield all eight states even though the usual assumption of direct dissociation, the "axial recoil" approximation, breaks down for three of the dication electronic states seen in the experiment.

DOI: 10.1103/PhysRevA.98.053429

I. INTRODUCTION

Theoretical and experimental interest in single-photon double photoionization is motivated by the fact that this process is exquisitely sensitive to the effects of electron correlation. For that reason, one-photon double ionization is the focus of an extensive literature, of which a small sample includes experimental studies on atoms [1–9] and molecules [10–19] and theoretical studies on atoms [20–41] that form the basis for theoretical treatments of the more challenging single-photon double photoionization from molecules [42–56]. In molecular targets, the physics of double photoionization and, in particular, its sensitivity to the role of electron correlation, is by far best revealed by measurements in the molecular frame [11–18], with no averaging over orientations of the molecule, but those measurements have been almost exclusively limited to the cases of the H_2 and D_2 molecules. One-photon double photoionization of H_2 is followed promptly by the Coulomb explosion of the H_2^{2+} dication, and a coincidence measurement of the momenta of the two ejected electrons and one of the protons (together with momentum conservation) produces a kinematically complete description of the double ionization and breakup process. This technique permits reconstruction of the molecular geometry at the time of photoionization, assuming a vertical electronic transition, and allows the observation of the triply differential cross section (TDCS) in the molecular frame.

Naturally, even more can be learned about this fundamental process with more complicated molecular targets, such as the other diatomic molecules of the first row elements, which could expose the role of electron correlation in double ionization of many-electron molecules. However the ground states and first few excited states of N_2^{2+} and O_2^{2+}, for example, have barriers to dissociation such that measurements are feasible only for double ionization producing higher-lying excited states of the dications. Thus the TDCS for double ionization to produce the ground and low-lying states of those dications, which would be the most accessible to sophisticated theoretical treatments like those that have been performed for H_2 and atoms, are not currently accessible by particle coincidence methods. Nonetheless, measurements of the TDCS for double photoionization of N_2 have been performed for randomly oriented molecules by Bolognesi *et al.* [19] producing results suggestive of the rich physics that lies behind this process in more complicated molecules. Moreover, measurement of the TDCS in the body frame of a nonlinear polyatomic molecule could provide insight into double photoionization uncomplicated by degeneracies in the states of the dication being produced. However, such a measurement requires a target molecule that dissociates upon double photoionization in such a way as to allow the complete determination of the body frame from the final momenta of the ions produced and observed in coincidence with the photoelectrons.

Here we explore the dissociation dynamics of doubly ionized water, a polyatomic molecule that provides a practical target for particle coincidence studies of double photoionization. With the aid of the complete nuclear dynamics we present here, the TDCS can be measured in the molecular frame for double ionization leading to the formation of eight of the lowest nine states of the H_2O^{2+} dication. This study focuses on the nuclear dynamics on the potential surfaces of the nine

*cwmccurdy@ucdavis.edu

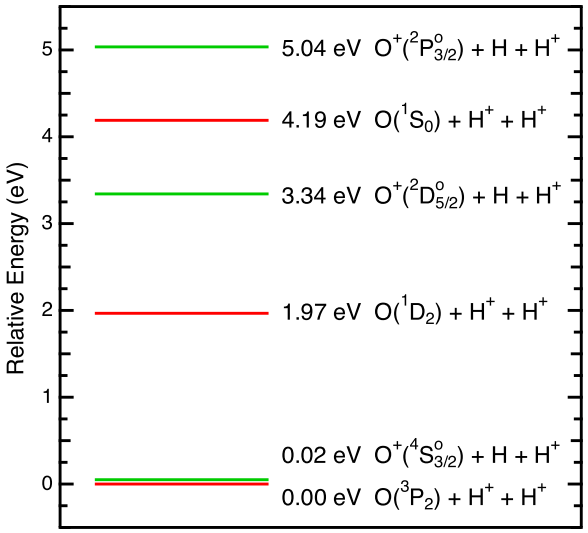

FIG. 1. Experimental energies of the low-energy asymptotes of the three-body breakup of H_2O^{2+} relative to the lowest state $O\,(^3P_2) + H^+ + H^+$ [58].

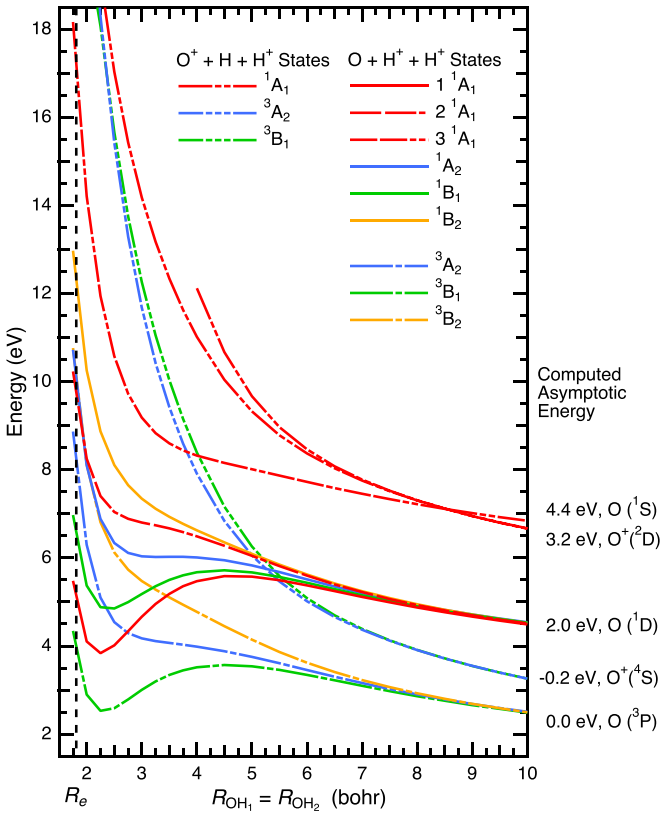

FIG. 2. Potential curves for the symmetric breakup ($\theta_{HOH} = 104.45^\circ$), $H_2O^{2+} \rightarrow O + H^+ + H^+$ and $O^+ + H + H^+$ from internally contracted multireference configuration interaction (icMRCI) calculations, showing the nine states of the water dication that correlate with the valence states of the oxygen atom and four of the valence states that correlate with the oxygen atomic ion. The energies given on the right-hand side of the figure indicate the computed asymptotic energies for the three particle breakup with the indicated atomic O state and the H atom, if present, in its ground state. The energies on the vertical scale on the left and the asymptotic energies on the right are relative to the $O(^3P) + H^+ + H^+$ asymptotic energy.

lowest states of H_2O, for eight of which the breakup channel producing two protons, $\gamma + H_2O \rightarrow 2H^+ + 2e^- + O$, either dominates or occurs to an experimentally measurable extent. We compare the results of our classical trajectory study with exploratory experiments using the cold target recoil momentum imaging method (COLTRIMS) that have recently yielded a complete momentum plane picture of the final momenta of the protons after double ionization yielding particular states of H_2O^{2+}. Those experimental results, including some preliminary observations of the photoelectrons that yield information about the electron dynamics, are reported in full detail in Ref. [57], hereafter referred to as Paper II.

The energies of the three-body breakup asymptotes of the H_2O^{2+} ion are given in Fig. 1. The lowest three electronic energy terms of the oxygen atom in its ground-state electronic configuration of $1s^2\,2s^2\,2p^4$ are the ^3P, ^1D, and ^1S levels whose degenerate components (neglecting spin-orbit coupling) comprise three triplet and six singlet states. When combined with two protons, these atomic states correlate with the nine lowest states of the H_2O^{2+} dication at the equilibrium geometry, as shown in Fig. 2. There are thus three energetic asymptotes for the process $H_2O^{2+} \rightarrow H^+ + H^+ + O$ for the nine lowest states of the dication. Additionally, there are low-energy asymptotes of the form $H + H^+ + O^+$. The two lowest such asymptotes have the oxygen ion in either its ground state O^+ (^4S) or in its first excited state O^+ (^2D). Note that at the equilibrium geometry these states are above the nine states that connect with the $H^+ + H^+ + O$ asymptotic states. However, as seen in Fig. 2, the states leading to $H + H^+ + O^+$ (^2D) cross the state of the same symmetry leading to the $H^+ + H^+ + O$ (^1S) asymptote, although these crossings occur at fairly large separations and, as will be discussed below, are not believed to affect the nuclear dynamics on the states leading to the $H^+ + H^+ + O$ asymptotes.

Figure 2 suggests that the nuclear dynamics for breakup of the dication might be direct, with the two protons dissociating roughly along the OH bonds for some channels and perhaps surmounting barriers to do so for the others. However the dynamics on the full potential surfaces shows that the dynamics of three-body breakup on some of these states is substantially more complicated. The axial recoil approximation, in which the dissociation of the dication is assumed to be direct and to occur before any appreciable rotation or rearrangement of the molecule (commonly used in the interpretation of momentum imaging experiments using the COLTRIMS method) breaks down radically for some of these electronic states. Nonetheless, a quantitative understanding the nuclear dissociation dynamics opens the door to four-particle coincidence measurements detecting two protons (which can establish the molecular frame) and two electrons that will constitute the TDCS in the molecular frame of a polyatomic molecule for eight of the nine states of the water dication dissociating to the lowest three energy levels of the oxygen atom.

The outline of this paper is as follows. In Sec. II we describe the potential surfaces, including the calculation of the surface for the $3\,^1A_1$ state, for the nine electronic states of the H_2O^{2+} dication on which we have carried out classical

trajectory studies. In Sec. III we discuss intersections occurring between the highest of those states and states correlating with other asymptotes. Section IV describes the classical trajectory study which sampled initial conditions from the Wigner phase-space distribution of neutral water in its ground state, and in Sec. V the results are compared with experimental measurements from Paper II to establish that the calculated dynamics are indeed consistent with the momentum plane observations. In Sec. VI we summarize how the knowledge of the nuclear dynamics, including for those channels in which the dissociation is not direct and for which the "axial recoil" approximation does not hold, can be used together with experimental observations to measure the TDCS in the body frame.

II. ELECTRONIC STATES OF H_2O^{2+}

At the equilibrium geometry of H_2O, the lowest nine electronic states of the water dication can be described qualitatively as the states that arise from the removal of two electrons from the highest three molecular orbitals of the Hartree-Fock ground-state electronic configuration, $1a_1^2\ 2a_1^2\ 1b_2^2\ 3a_1^2\ 1b_1^2$. As shown in Fig. 2, for three-body breakup the $^3B_1$, $^3A_2$, and $^3B_2$ states correlate with the three components of the ^3P ground state of the oxygen atom. The $1\,^1A_1$, $^1B_1$, $2\,^1A_1$, $^1A_2$, and $^1B_2$ correlate with the components of the ^1D state of oxygen. The $3\,^1A_1$ correlates with the oxygen ^1S state.

In a study of the breakup of the water dication into the $H^+ + OH^+$ channel, Gervais *et al.* [59] computed potential surfaces for the eight states dissociating to the O ^3P and ^1D states. Those surfaces were calculated at a sophisticated level using internally contracted multireference configuration interaction (icMRCI) methods at the configuration interaction singles and doubles (CISD) level including the Davidson correction for quadruple excitations. Those accurate *ab initio* surfaces were fit to a linear combination of 100 basis functions that represent the Coulomb and polarization interactions at intermediate and long interatomic distances together with screened Coulomb and multipole interactions at short distances. The typical deviation of the fit, which is described in detail in Ref. [59], from the calculated energy points was of the order of 10^{-3} hartrees in that study, and the fits represent the surface for $R_{OH} > 0.8$ bohr and $\theta > 80°$. We used those surfaces for the lower eight states in the classical trajectory calculations we report here.

Since our interest is in three-body breakup of the dication, and since the preliminary experiments in Paper II observed all three asymptotes, we calculated the remaining potential surface for the $3\,^1A_1$ state, and used the functional form developed by Gervais *et al.* to fit it. The calculations were performed with the MOLPRO [60,61] suite of quantum chemistry programs using the same icMRCI method at the CISD level including the Davidson correction as the calculations of the other surfaces [59] employed in the classical trajectory calculations in Sec. IV. The Gaussian basis was the *cc-p*VTZ Dunning correlation consistent basis [62], and the MRCI calculations were based on orbitals from complete active-space self-consistent field (CASSCF) calculations on the lowest $^3B_1$ state in C_s symmetry with one a' orbital frozen and six electrons in five a' and two a'' orbitals. The grid of

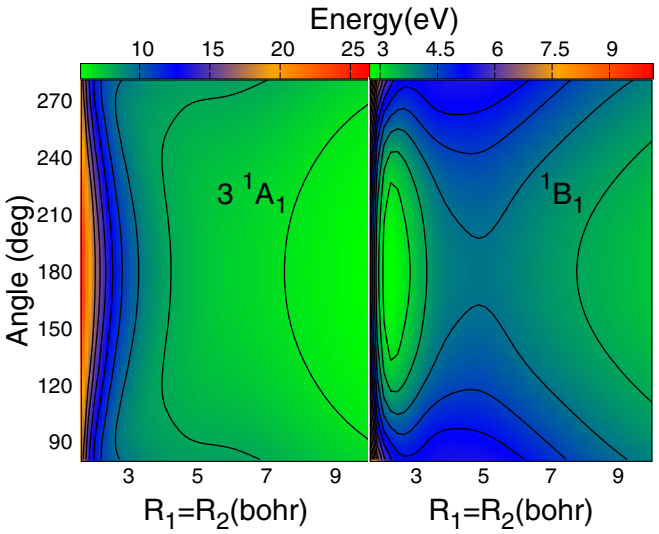

FIG. 3. Comparison of $3\,^1A_1$ and $^1B_1$ potential surfaces as a function of symmetric stretch and HOH angle.

4722 geometries consisted of 11 angles from 80° to 180° and values of R_{OH} from 1 to 50 bohrs with fine spacings at short distances.

Two comparisons of potential surfaces relevant to the dynamics in the three-body breakup channel to produce two protons are shown in Figs. 3 and 4. As we will see below in Sec. V, dissociation into the $O + H^+ + H^+$ arrangement is direct for some of the nine states of the dication we consider. For these dication states, the axial recoil approximation is valid and the final momenta of the two protons can be used in a COLTRIMS experiment to determine the plane of the molecule and its orientation in coincidence with the photoelectrons. But for others, in particular for the $^1B_1$ state shown in those figures, the axial recoil approximation breaks down completely, but does so in a predictable way that potentially

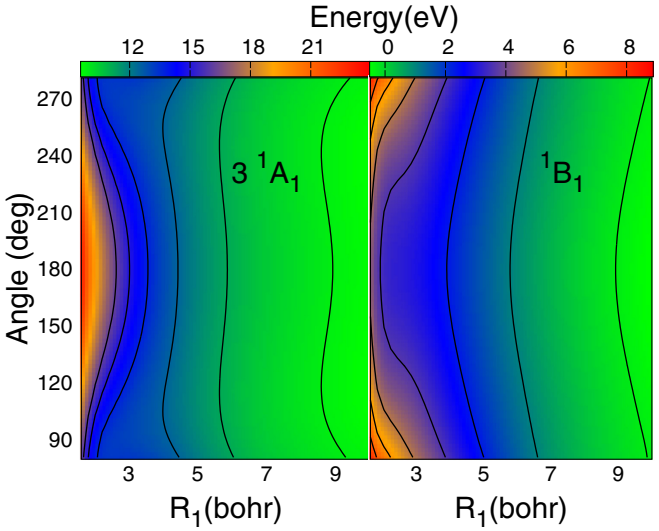

FIG. 4. Comparison of $3\,^1A_1$ and $^1B_1$ potential surfaces as a function one R_{OH} distance and HOH angle with the other internuclear distance fixed at $R_{OH} = 1.81$ bohrs.

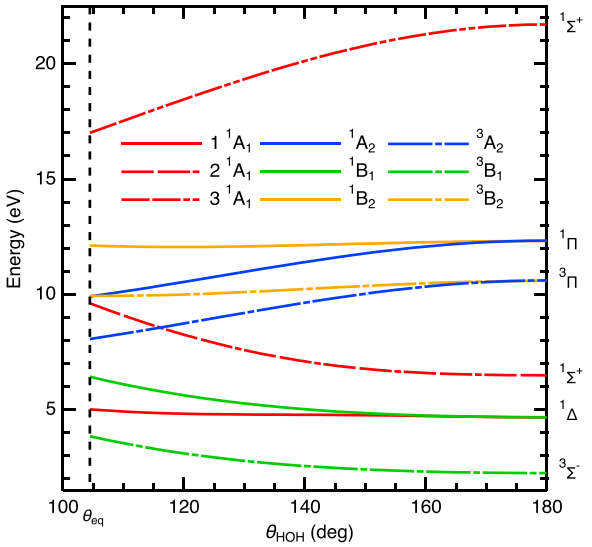

FIG. 5. Potential curves for bending with $R_{OH} = 1.81$ bohrs from multireference CISD calculations for the nine states of the water dication that correlate with the valence states of the oxygen atom (see Fig. 2).

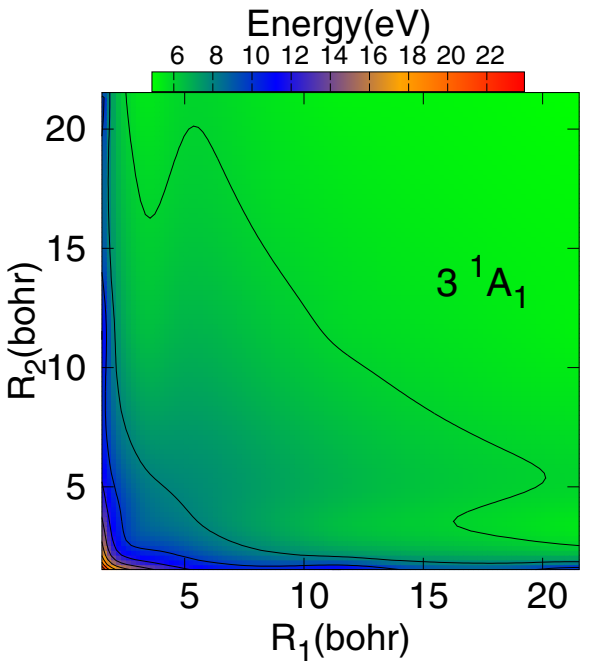

FIG. 6. Calculated potential surface as a function of R_{OH} distances with $\theta = 104.45°$ showing the shallow OH^+ well and barrier to dissociation.

allows the determination of the molecular frame. For both the $3\ ^1A_1$ and $^1B_1$, a strong gradient towards symmetric dissociation is visible in Fig. 3 that is reflected also in the curves in Fig. 2. The key difference between the two potential surfaces is visible at the left-hand edges of each panel of Figs. 3 and 4 where there is a strong gradient towards larger bond angles in the case of the $^1B_1$ state while the opposite is the case for the $3\ ^1A_1$. In Fig. 5 we plot bending curves on the nine surfaces with the OH distances fixed at the equilibrium distance of the neutral and where the behavior of the $3\ ^1A_1$ and $^1B_1$ states contrasts strongly. We can make the simple observation that at the equilibrium geometry the potential surfaces of three of the states, the $^3B_1$, $^1B_1$, and $2\ ^1A_1$ have a strong or significant component of the gradient in the direction of larger bond angles. That observation is directly correlated with the breakdown of the axial recoil approximation that we see in the classical trajectory study of the three-body breakup channel.

We note that similar calculations of portions of the potential surfaces carried out using uncontracted multireference CISD and larger complete active-space (CAS) choices with the COLUMBUS suite of quantum chemistry programs [63–65] gave no significant differences with the calculations used to compute the complete surfaces for dynamics. For example, the calculations that generated the curves in Figs. 2 and 5 were also carried out with a larger CAS space in the MCSCF and larger reference space for the CISD calculation that consisted of three a_1, two b_1, two b_2, and one a_2 active orbitals (with the $1a_1$ orbital frozen) and show only inconsequential overall energy shifts from the less-correlated calculations.

Finally we observe that the $OH^+ + H^+$ asymptote of the potential surface for the $3\ ^1A_1$ ($4\ ^1A'$) state is the $^1\Sigma^+$ state with a dominant configuration $1\sigma^2\ 1\pi^4\ 2\sigma^2$ which is not bound but has a barrier to symmetric dissociation, apparent in Fig. 6, of about 0.56 eV. In our study, none of the classical trajectories in the ensemble were observed to remain trapped behind the barrier.

III. DIABATIC STATES LEADING TO $O^+ + H^+ + H$ ASYMPTOTES AND AN APPROXIMATE DIABATIC SURFACE FOR THE $3\ ^1A_1$ STATE

In the present paper we are comparing to experiments [57] performed at a photon energy of 57 eV, which corresponds to 20.3 eV on the energy scale used in Fig. 2. At this energy the states that are diabatically connected to the $O^+ + H^+ + H$ asymptotes are not energetically accessible. However, we know from the asymptotes, illustrated in Fig. 1, that the diabatic states of $^1A'$ symmetry leading the $O^+(^2D^o_{5/2}) + H + H^+$ must cross the $^1A'$ state, which has $^1A_1$ symmetry in C_{2v} geometries, that is connected to $O(^1S_0) + H^+ + H^+$. To calculate the potential-energy surfaces (PESs) that are diabatically connected to both O^+ and O asymptotes we have performed icMRCI calculations based on orbitals from a state-average (SA) CASSCF reference wave function that had two $^3B_1$, two $^3A_2$, and one $^3B_1$ reference states. As can be seen in Fig. 2, these reference states include states that are connected to both O^+ and O asymptotes.

Additionally, we can see in Fig. 2 that the PESs that correlate to the $O^+(^4S)$ asymptote do not cross any of the lower triplet states correlating to the ^3P of neutral oxygen atoms. However, the PESs that correlate to the $O^+(^2D)$ asymptote cross the $3\ ^1A_1$ PES at 8.5 bohrs. Additional insight into these different PESs is given by considering cuts of the eight lowest $^1A'$ PESs with fixed $\theta = 110°$ and constant $R_{OH_1} + R_{OH_2} = 14.75$ a.u. shown in Fig. 7. The diabats shown there were constructed by sorting the fixed-nuclei energies into sets that gave the smoothest connected curves. We note that there was an exceedingly small energy splitting found where the states connected to the different asymptotes crossed. The very weak interactions between the diabats is presumably due to the fact

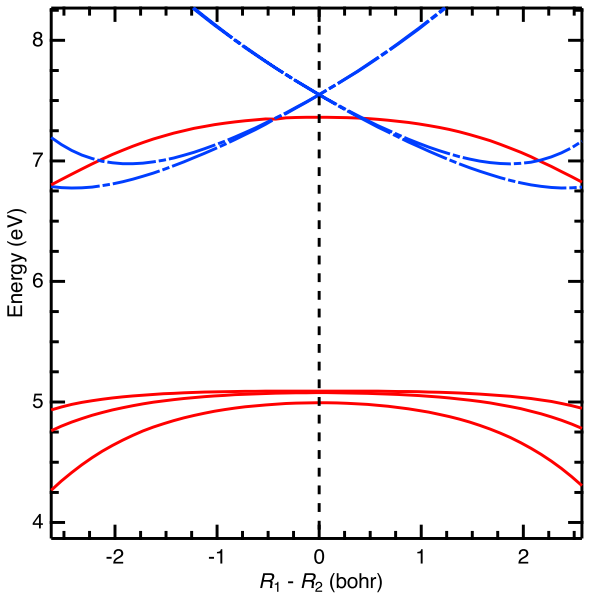

FIG. 7. Cuts through the icMRCI diabatic PESs for the lowest eight A' states of H_2O^{2+} for $\theta = 110^\circ$ with $R_{OH_1} + R_{OH_2} = 14.75$ bohrs. The solid red lines are for the PESs that diabatically connect to the $O + H^+ + H^+$ asymptotes and the dashed blue lines are for the PESs that diabatically connect to the $O^+ + H^+ + H$ asymptotes.

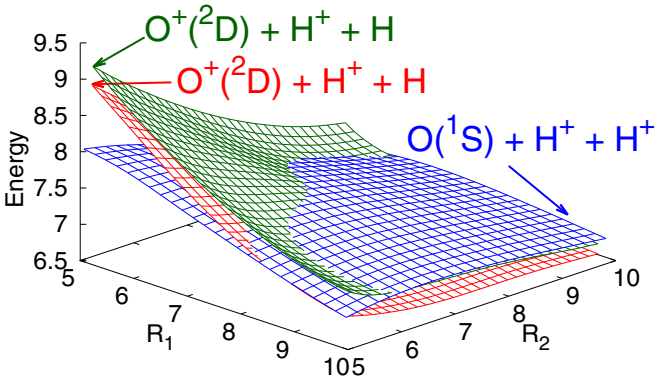

FIG. 8. Calculated PESs in eV as a function of R_1(bohr) and R_2(bohr) distances with $\theta = 110^\circ$. The red and green surfaces are the fifth and sixth adiabatic states of $^1A'$ symmetry in the icMRCI calculation based on five states in the SA-CASSCF calculation. The blue surface is the potential that was fit to the converged icMRCI points where the fourth $^1A'$ could be well described as being connected to the $O(^1S) + H^+ + H^+$ asymptote. This approximate diabat for the $3\,^1A_1$ state passes through the two surfaces that correlate to $O^+(^2D)$ state.

that any such splitting would be caused by the tunneling of an electron from an O atom to a proton at a distance of over 7 bohrs.

The choice of CASSCF reference wave function in the computation of the potential surface for the $3\,^1A_1$ state used to study the breakup dynamics included only one state, the $^3B_1$ ground state. This reference space could adequately represent states with the $O + H^+ + H^+$ asymptote but was insufficient for converging the icMRCI calculations using MOLPRO for states dominated by configurations describing the $O^+ + H^+ + H$ asymptote. Thus there was a subset of geometries where the icMRCI did not converge to a $3\,^1A_1$ state with a strong overlap with the reference space. This potential was then fit using the analytical form of Gervais *et al.* [59] neglecting points at those geometries and incorporating the proton-proton repulsion at large distances.

As seen in Fig. 8, the choice of the $^3B_1$ state as the reference wave function coupled with the assumptions made in the fitting procedure provided an approximate diabat for the $3\,^1A_1$ state. This approximate diabatic surface allowed the calculation of classical trajectories leading to the $O + H^+ + H^+$ asymptote neglecting the effects of small couplings to states leading to the other arrangements.

IV. CLASSICAL TRAJECTORIES SAMPLING FROM THE INITIAL VIBRATIONAL DISTRIBUTION OF NEUTRAL H_2O

We have calculated ensembles of classical trajectories for each state of the dication, sampling from the Wigner phase-space distribution for the normal modes of vibration of the neutral water molecule. The Wigner distribution [66] is a semiclassical phase distribution that can provide a useful ensemble of initial conditions for classical trajectories that approximately represent the effects of zero-point motion. For the harmonic oscillator, it is given by a familiar and everywhere positive analytical expression. For a molecule with N atoms the Wigner distribution in the harmonic approximation is

$$W(\mathbf{Q},\mathbf{P}) = \frac{1}{(\pi\hbar)^{3N-6}} \prod_{j=1}^{3N-6} \exp\left[-\frac{\omega_j}{\hbar} Q_j^2 - \frac{P_j^2}{\hbar\omega}\right], \quad (1)$$

where Q_j and P_j are the normal-mode coordinates and momenta, respectively, and ω_j are the associated frequencies which are defined in terms of the eigenvectors and eigenvalues of the mass weighted Hessian, $B_{i,j} = (m_i m_j)^{-1/2} \partial^2 V / \partial x_i \partial x_j$,

$$\mathbf{BL} = \mathbf{L\Lambda}, \quad (2)$$

with $\mathbf{L}^T\mathbf{L} = \mathbf{1}$ and $\Lambda_j = \omega_j^2$. Metropolis sampling of Eq. (1) can be used to provide initial conditions for the classical trajectories in the original Cartesian coordinates and momenta, x_i and p_i, according to

$$x_i = x_i^{(0)} + \frac{1}{\sqrt{m_i}} \sum_{j=1}^{3N-6} L_{i,j} Q_j,$$

$$p_i = \sqrt{m_i} \sum_{j=1}^{3N-6} L_{i,j} P_j. \quad (3)$$

Such an ensemble of initial conditions provides a classical approximation to the quantum dissociation dynamics initiated by an electronic transition to the double continuum governed by the Franck-Condon approximation.

Here we used the normal modes from a CASSCF calculation on neutral H_2O using the same CAS choice and basis as in the calculations on the excited-state ions. The calculated normal-mode frequencies were 3762.7, 1692.8, and

TABLE I. Branching ratios for three-body breakup channel from ensembles of 1000 classical trajectories with initial conditions sampled from the Wigner distribution of the initial neutral state.

H_2O^{2+} electronic state	% three-body $O + 2H^+$	Axial recoil breakdown
$^3B_1$	7.6	yes
$1\,^1A_1$	1.6	
$^1B_1$	15.4	yes
$2\,^1A_1$	67.5	yes
$^3A_2$	100	no
$^3B_2$	99.8	no
$^1A_2$	99.6	no
$^1B_2$	99.1	no
$3\,^1A_1$	100	no

3877.9 cm^{-1}, which are 3–6% larger than the experimental values. Gervais *et al.* [59] performed a similar sampling of the Wigner distribution in their study of the OH^+/H^+ dissociation channel, but used the experimental values of the frequencies instead of the computed ones. The branching ratios into the three-body arrangement from calculations using ensembles of 1000 trajectories are shown in Table I. The criterion for categorizing a trajectory as three body was that the R_{OH} distance of one proton be 200 bohrs or greater and that the other reach at least 50 bohrs.

The calculated branching ratios generally reproduce the trends in the calculations of Gervais *et al.* for dissociation of the first eight of these states in the case of HOD^{2+}. They point out that the branching ratios are controlled in large measure by saddle points at equal values of the R_{OH} distance in the potential surfaces of the lower four states. Those branching ratios show a strong isotope effect and may also be sensitive to the details of the distribution of initial conditions.

V. FINAL MOMENTUM DISTRIBUTIONS FOR THREE-BODY BREAKUP AND THE BREAKDOWN OF THE AXIAL RECOIL APPROXIMATION

Here we make two comparisons with a portion of the preliminary experimental data that is presented and analyzed fully in Paper II [57] where the experimental methods are also described in detail. The first comparison is a plot of the kinetic-energy release (KER, the sum of kinetic energies of the atomic fragments) versus the angle between the final momenta of the two protons. As explained in Ref. [57], those data in the experiment can be separated by the final electronic state of the oxygen atom, since the two protons are observed in coincidence with the two electrons and the sum of these kinetic energies distinguishes the electronic state of the oxygen fragment. The experimental results analyzed in that way are shown in the lower row of Fig. 9 as a density plot that represents a histogram of coincidence counts. In the upper

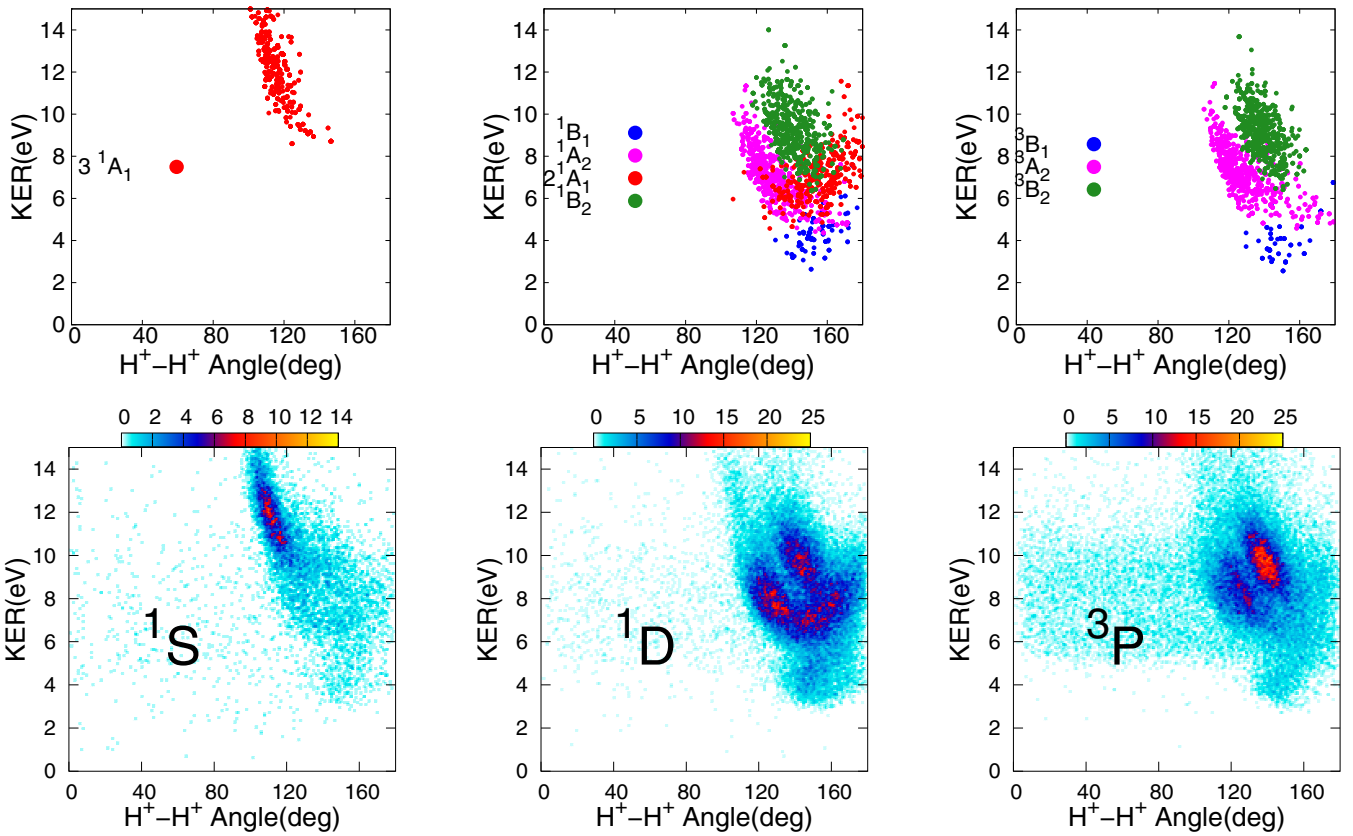

FIG. 9. Plots of the total kinetic-energy release of the atomic fragments vs the angle between the momenta of the ejected protons shown separately for the three states of the oxygen atom that can be distinguished in the experiment. Top row: classical trajectories; bottom row: histogram plot of experimental measurements.

panel, the asymptotic values for the kinetic-energy release and the angle between the proton momenta for the classical trajectories surviving into the three-body breakup channel are plotted as individual points.

The classical trajectory results in Fig. 9 show that the correlation between KER and H^+–H^+ angles can be used to identify initial states of the H_2O^{2+} ions that dominate in various regions of the plot. The agreement between the experimental and theoretical distributions in that figure demonstrates that this correlation can be used to perform that identification in other experiments in which the photoelectrons are observed in coincidence with the protons. For the purposes of measuring the TDCS for double photoionization, this analysis is key to the determination of which electronic state of the dication produced the two electrons measured in coincidence with the protons. There appears to be considerable correlation between the intensities of the features in the experimental observation and the density of classical trajectories in the upper panels of Fig. 9. However, the relative numbers of classical trajectories in each of the features is determined by the branching ratios to produce the three-body channel on each dication potential surface. Only if the total double photoionization cross sections were approximately the same in magnitude for all the states would one expect the classical trajectories alone to predict the relative intensities of the experimental features. Otherwise, it would be necessary to weight the classical trajectory intensities by the relative cross sections for double ionization to produce their respective dication states.

We note that the $1\,^1A_1$ state produces too few trajectories in the three-body breakup channel to appear in the plot that predicts the KER versus the angle between the ejected protons for states that correlate to the ^1D state of the oxygen atom. The fact that there are only four features in the experimental observation in the corresponding panel (bottom middle) of Fig. 9 is consistent with the theoretical prediction based solely on the branching ratio of the classical trajectories.

The comparison in the rightmost panels of Fig. 9 of classical trajectory and experimental distributions for the ^3P asymptote shows two strong and one weak feature in close agreement, but the experiment displays an additional broad distribution between KER values of about 5.5–10 eV and extending over all H^+–H^+ angles. We note that the Franck-Condon region for double ionization to produce the $2\,^1A_1$ state corresponds to at least the upper part of that range of KER, and correlates in the two-body channel, which it produces about 33% of the time (Table I), to the $b\,^1\Sigma^+$ state of OH^+. That state is known to be predissociated by an intersystem crossing with the $A^3\Pi$ of OH^+ [59,67] to produce $O(^3P) + H^+$ with a lifetime of on the order of 2 ps. It is reasonable therefore to speculate that this two-body dissociation channel could produce events in this fourth feature of the experimental distribution for the $O(^3P)$ three-body channel. Figure 2 suggests that a similar mechanism might connect both the $1\,^1A_1$ and $^1B_1$ states of H_2O^{2+} with the triplet three-body asymptote producing other events in this range of KER for which the axial recoil approximation would also break down.

The second comparison with the experiment described in Paper II [57] is shown in Fig. 10 where the final momenta of the protons from the classical trajectories for the $3\,^1A_1$ and the $1\,^1B_1$ are plotted. In a COLTRIMS experiment, in the absence of knowledge of the dissociation dynamics, the assumption of the axial recoil approximation can be used to determine the apparent orientation of the molecule and thus locate the directions of the ejected electrons in the body frame. The meaning of "axial recoil" approximation [68] in interpreting momentum coincidence experiments in the case of diatomics is the assumption that the fragments are ejected along the direction of vibration and that the axis of the molecule does not rotate appreciably before dissociation is complete. Here, for the dissociation of the triatomic water dication, strict "axial recoil" dynamics would mean that the two protons are ejected along the bond directions as indicated in the top left panel of Fig. 10. However, for the purposes of determining the initial orientation of the symmetry axis of the molecule in this case, it suffices that the two protons be ejected symmetrically near the original bond directions.

Thus in the analysis of the experimental data shown in Fig. 10, the bisector of the angle between the momenta of the two protons determines the z axis of the momentum plane, and the directions of the momenta of the protons are assigned equal angles above and below that axis. The momentum of the oxygen is deduced by momentum conservation under the assumption of a cold target with no center-of-mass momentum, and thus has the opposite sign for its z component. To the degree that the dissociation is direct and symmetric, this procedure determines the plane of the molecule and its orientation in that plane for the purposes of coincidence measurements with the ejected electrons. The final momenta of computed classical trajectories can be plotted in exactly the same way to allow a direct comparison with the experiment, and this is what is also shown in Fig. 10.

For the $3\,^1A_1$ state the comparison in Fig. 10 of classical trajectory results with experiment shows that the axial recoil approximation captures the majority of the physics of dissociation. Importantly, when the computed final momenta are plotted in the same way as the COLTRIMS experimental data they are little changed by the assumption of axial recoil. The agreement with the experimental data in this case is excellent.

However, for the $1\,^1B_1$ state the majority of the protons in the three-body channel emerge traveling towards the *opposite* side of the molecule from the one from which they originated, signaling the complete breakdown of the axial recoil approximation. The origin of this distinctive difference between the dissociation dynamics of the $1\,^1B_1$ and that of the $3\,^1A_1$ state is the strong gradient of the potential surface toward bond angle opening in the former case and the gradient toward bond angle closure in the latter. The contrast between these aspects of the two potential surfaces can be seen in Figs. 3–5 and was described in Sec. II.

To illustrate how the gradient in the potential surface affects the dissociation dynamics, a random selection of a subset of the trajectories on the $1\,^1B_1$ potential surface is plotted in Fig. 11, showing how they invert the sense of the original bond angle of the molecule. Nonetheless, when the classical trajectories are plotted in the same way as the experimental data, under the assumption of axial recoil as described above (center panels of Fig. 10), they reproduce the experimental momentum plane image (right panels of Fig. 10), verifying that the trajectories on this potential surface accurately represent the observed dissociation dynamics. Similar results are

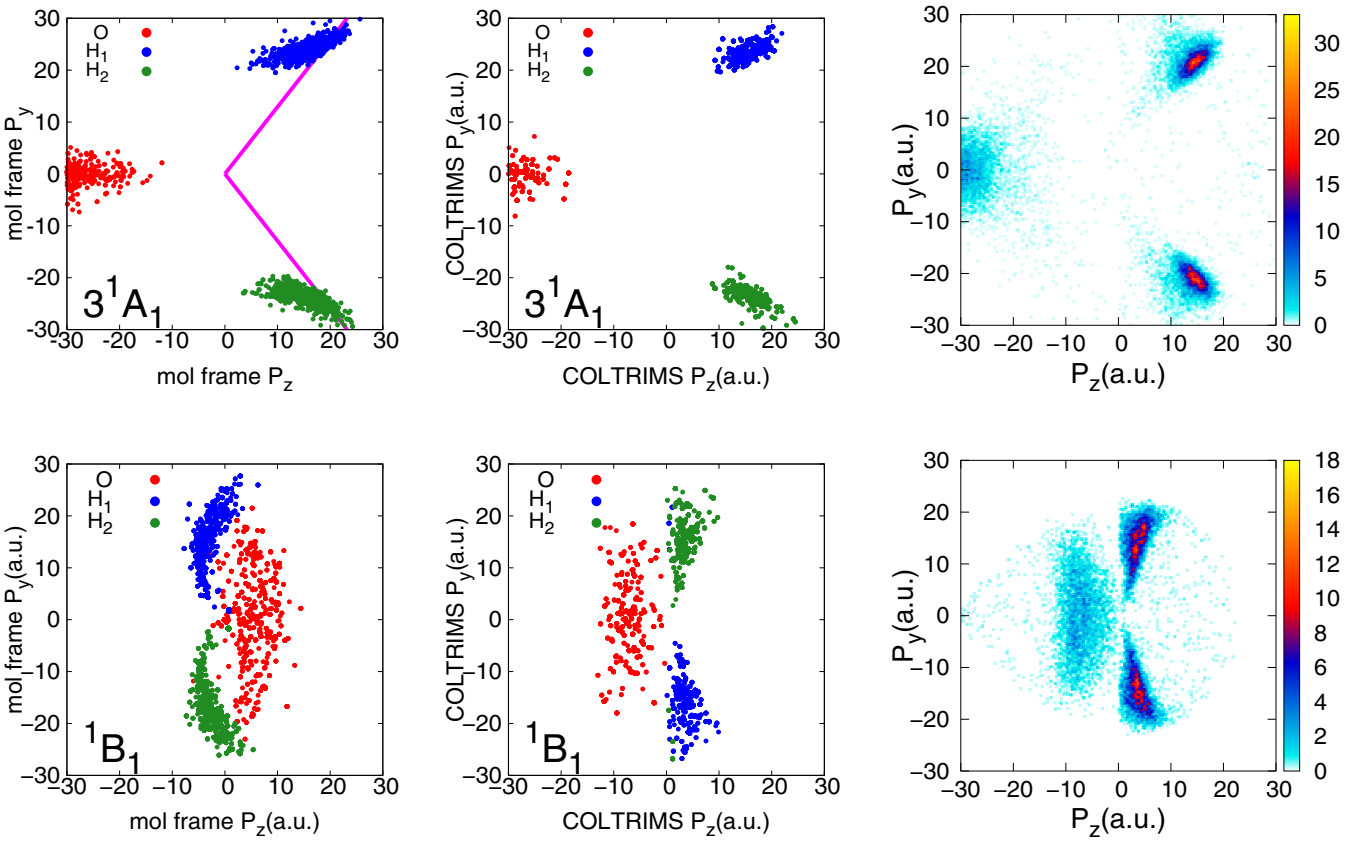

FIG. 10. Fragment momentum distributions for $3\,^1A_1$ and $^1B_1$. Left panels: computed final momenta of the classical trajectories; solid lines indicate directions of strict axial recoil dynamics. Middle panels: momenta from the classical trajectories analyzed and plotted to determine the apparent molecular plane and orientation under the assumption of axial recoil as explained in the text. Right panels: COLTRIMS experimental data analyzed and plotted as in the middle panels.

found for all three states ($^3B_1$, $^1B_1$, and $2\,^1A_1$) whose potential surfaces have a strong gradient towards bond opening, as shown in Fig. 5. We note in passing that similar scissoring dynamics that invert the sense of the bond angle have been observed in dissociative attachment of electrons to water to produce oxygen anions [69].

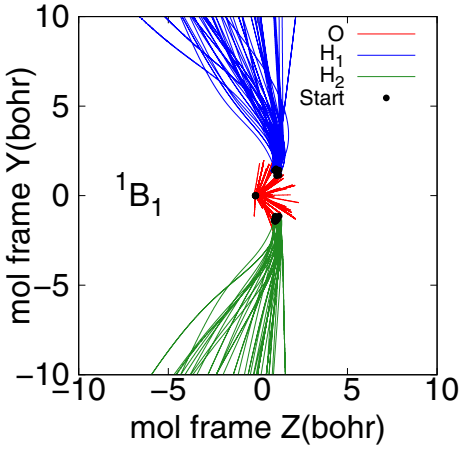

FIG. 11. Sixty randomly sampled trajectories in the three-body breakup channel of the $^1B_1$ potential surface, showing the inversion of the original bond angle and consequent breakdown of the axial recoil approximation.

Thus for the eight states that are evidently observed in the experiment, the three-body dissociation dynamics of five of these satisfy the axial recoil approximation, while for the other three, the axial recoil approximation breaks down completely, but does so in a particularly simple and potentially nonetheless useful way. The lower panels of Fig. 10 illustrate a mapping of the experimental results analyzed under the assumption of axial recoil onto the correct momentum plane. The classical trajectory results allow the isolation of parts of the experimental observations that are dominated by trajectories that unambiguously invert the original plane of the molecule.

VI. CONCLUSION

We have verified that the three-body dissociation dynamics of the water dication for the states that dissociate to the oxygen atom in its ^3P, ^1D, and ^1S states and two protons are well described by classical trajectories on the computed potential-energy surfaces. The theoretical calculations predict the momentum plane distributions of the final states in good agreement with preliminary experimental data, and open the way for a full experimental determination of the TDCS in the body frame for one-photon double photoionization of the water molecule. A complete comparison of theory and

experiment for the remaining six states, not shown here, is given in Paper II [57].

We have found that for three of those dication electronic states the axial recoil approximation, which has been the basis for the interpretation of most COLTRIMS experiments, and which previously seemed essential to the construction of body frame information from coincidence measurement of ions and photoelectrons, breaks down radically. Nonetheless the analysis in Sec. V will potentially allow the measurement of the TDCS in the body frame for those states as well. Those experiments have the potential to reveal the details of double photoionization in the body frame of a polyatomic molecule.

Experiments such as these will pose a profound challenge to theory to predict the body-frame TDCS for double photoionization of water. The current state of the art for *ab initio* calculation of double photoionization amplitudes is to treat the dynamics of two active electrons completely while freezing the others in target atomic or molecular orbitals. Such calculations have only been carried out on atoms [33,38–41,70–72] to our knowledge, but in those cases surprisingly good agreement with experimental angular distributions of the ejected electrons was obtained. To calculate the TDCS for one-photon double ionization of water, we can make the same two-active-electron approximation, and use the computational methods involving a single center expansion and numerical grids that we have used previously in double photoionization calculations on H_2 [47–50]. This approach promises to accurately describe correlation between the two outgoing electrons. A critical open question is whether the approximation of treating only two active electrons will be sufficient to describe the effects of initial-state correlation on the removal of two electrons from the same orbital as well as from different orbitals of the neutral molecule to produce different states of the dication.

ACKNOWLEDGMENTS

Work at LBNL was performed under the auspices of the U.S. Department of Energy (DOE) under Contract No. DE-AC02-05CH11231 and was supported by the U.S. DOE Office of Basic Energy Sciences, Division of Chemical Sciences. Calculations presented here made use of the resources of the National Energy Research Scientific Computing Center, a DOE Office of Science User Facility. F.L.Y. was supported by the National Science Foundation, Grant No. PHY-1509971, and the U.S. DOE Office of Science, Office of Workforce Development for Teachers and Scientists (WTDS) under the Visiting Faculty Program.

[1] L. Avaldi and A. Huetz, J. Phys. B **38**, S861 (2005).
[2] O. Schwarzkopf, B. Krässig, J. Elmiger, and V. Schmidt, Phys. Rev. Lett. **70**, 3008 (1993).
[3] R. Dörner, T. Vogt, V. Mergel, H. Khemliche, S. Kravis, C. L. Cocke, J. Ullrich, M. Unverzagt, L. Spielberger, M. Damrau, O. Jagutzki, I. Ali, B. Weaver, K. Ullmann, C. C. Hsu, M. Jung, E. P. Kanter, B. Sonntag, M. H. Prior, E. Rotenberg *et al.*, Phys. Rev. Lett. **76**, 2654 (1996).
[4] R. Dörner, J. M. Feagin, C. L. Cocke, H. Bräuning, O. Jagutzki, M. Jung, E. P. Kanter, H. Khemliche, S. Kravis, V. Mergel, M. H. Prior, H. Schmidt-Böcking, L. Spielberger, J. Ullrich, M. Unversagt, and T. Vogt, Phys. Rev. Lett. **77**, 1024 (1996).
[5] R. Dörner, H. Bräuning, J. M. Feagin, V. Mergel, O. Jagutzki, L. Spielberger, T. Vogt, H. Khemliche, M. H. Prior, J. Ullrich, C. L. Cocke, and H. Schmidt-Böcking, Phys. Rev. A **57**, 1074 (1998).
[6] L. Malegat, P. Selles, P. Lablanquie, J. Mazeau, and A. Huetz, J. Phys. B **30**, 263 (1997).
[7] H. Bräuning, R. Dörner, C. L. Cocke, M. H. Prior, B. Krässig, A. S. Kheifets, I. Bray, A. Bräuning-Demian, K. Carnes, S. Dreuil, V. Mergel, P. Richard, J. Ullrich, and H. Schmidt-Böcking, J. Phys. B **31**, 5149 (1998).
[8] S. Cvejanovic, J. P. Wightman, T. J. Reddish, F. Maulbetsch, M. A. MacDonald, A. S. Kheifets, and I. Bray, J. Phys. B **33**, 265 (2000).
[9] P. Bolognesi, V. Feyer, A. Kheifets, S. Turchini, T. Prosperi, N. Zema, and L. Avaldi, J. Phys. B **41**, 051003 (2008).
[10] T. J. Reddish, J. P. Wightman, M. A. MacDonald, and S. Cvejanović, Phys. Rev. Lett. **79**, 2438 (1997).
[11] R. Dörner, H. Bräuning, O. Jagutzki, V. Mergel, M. Achler, R. Moshammer, J. M. Feagin, T. Osipov, A. Bräuning-Demian, L. Spielberger, J. H. McGuire, M. H. Prior, N. Berrah, J. D. Bozek, C. L. Cocke, and H. Schmidt-Böcking, Phys. Rev. Lett. **81**, 5776 (1998).
[12] D. P. Seccombe, S. A. Collins, T. J. Reddish, P. Selles, L. Malegat, A. K. Kazansky, and A. Huetz, J. Phys. B **35**, 3767 (2002).
[13] T. Weber, A. Czasch, O. Jagutzki, A. Müller, V. Mergel, A. Kheifets, J. Feagin, E. Rotenberg, G. Meigs, M. H. Prior, S. Daveau, A. L. Landers, C. L. Cocke, T. Osipov, H. Schmidt-Böcking, and R. Dörner, Phys. Rev. Lett. **92**, 163001 (2004).
[14] T. Weber, A. O. Czasch, O. Jagutzki, A. K. Muller, V. Mergel, A. Kheifets, E. Rotenberg, G. Meigs, M. H. Prior, S. Daveau, A. Landers, C. L. Cocke, T. Osipov, R. Diez Muino, H. Schmidt-Bocking, and R. Dorner, Nature (London) **431**, 437 (2004).
[15] T. Weber, L. Foucar, T. Jahnke, M. Schoeffler, L. Schmidt, M. Prior, and R. Doerner, J. Phys. B **50**, 164002 (2017).
[16] T. Weber, A. O. Czasch, O. Jagutzki, A. K. Muller, V. Mergel, A. Kheifets, E. Rotenberg, G. Meigs, M. H. Prior, S. Daveau, A. Landers, C. L. Cocke, T. Osipov, R. Diez Muino, H. Schmidt-Bocking, and R. Dorner, Nature (London) **443**, 1014 (2006).
[17] M. Gisselbrecht, M. Lavollée, A. Huetz, P. Bolognesi, L. Avaldi, D. P. Seccombe, and T. J. Reddish, Phys. Rev. Lett. **96**, 153002 (2006).
[18] D. Akoury, K. Kreidi, T. Jahnke, T. Weber, A. Staudte, M. Schöffler, N. Neumann, J. Titze, L. P. H. Schmidt, A. Czasch, O. Jagutzki, R. A. C. Fraga, R. E. Grisenti, R. D. Muiño, N. A. Cherepkov, S. K. Semenov, P. Ranitovic, C. L. Cocke, T. Osipov, H. Adaniya *et al.*, Science **318**, 949 (2007).
[19] P. Bolognesi, B. Joulakian, A. A. Bulychev, O. Chuluunbaatar, and L. Avaldi, Phys. Rev. A **89**, 053405 (2014).
[20] F. Maulbetsch and J. S. Briggs, J. Phys. B **28**, 551 (1995).
[21] F. Maulbetsch and J. S. Briggs, J. Phys. B **27**, 4095 (1994).
[22] A. S. Kheifets and I. Bray, Phys. Rev. A **54**, R995 (1996).
[23] S. P. Lucey, J. Rasch, C. T. Whelan, and H. R. J. Walters, J. Phys. B **31**, 1237 (1998).
[24] A. S. Kheifets and I. Bray, J. Phys. B **31**, L447 (1998).
[25] A. S. Kheifets and I. Bray, Phys. Rev. A **57**, 2590 (1998).

[26] J. S. Briggs and V. Schmidt, J. Phys. B **33**, R1 (2000).
[27] L. Malegat, P. Selles, and A. Huetz, J. Phys. B **30**, 251 (1997).
[28] P. Selles, L. Malegat, and A. K. Kazansky, Phys. Rev. A **65**, 032711 (2002).
[29] C. W. McCurdy, D. A. Horner, T. N. Rescigno, and F. Martín, Phys. Rev. A **69**, 032707 (2004).
[30] D. A. Horner, J. Colgan, F. Martín, C. W. McCurdy, M. S. Pindzola, and T. N. Rescigno, Phys. Rev. A **70**, 064701 (2004).
[31] J. Colgan, M. S. Pindzola, and F. Robicheaux, Phys. Rev. A **72**, 022727 (2005).
[32] M. S. Pindzola, F. Robicheaux, S. D. Loch, J. C. Berengut, T. Topcu, J. Colgan, M. Foster, D. C. Griffin, C. P. Ballance, D. R. Schultz, T. Minami, N. R. Badnell, M. C. Witthoeft, D. R. Plante, D. M. Mitnik, J. A. Ludlow, and U. Kleiman, J. Phys. B **40**, R39 (2007).
[33] D. C. Griffin, M. S. Pindzola, C. P. Ballance, and J. Colgan, Phys. Rev. A **79**, 023413 (2009).
[34] A. S. Kheifets, D. V. Fursa, C. W. Hines, I. Bray, J. Colgan, and M. S. Pindzola, Phys. Rev. A **81**, 023418 (2010).
[35] M. S. Pindzola, C. P. Ballance, S. A. Abdel-Naby, F. Robicheaux, G. S. J. Armstrong, and J. Colgan, J. Phys. B **46**, 035201 (2013).
[36] Y. Li, M. S. Pindzola, and J. Colgan, J. Phys. B **49**, 195205 (2016).
[37] F. L. Yip, D. A. Horner, C. W. McCurdy, and T. N. Rescigno, Phys. Rev. A **75**, 042715 (2007).
[38] F. L. Yip, T. N. Rescigno, and C. W. McCurdy, Phys. Rev. A **94**, 063414 (2016).
[39] F. L. Yip, T. N. Rescigno, C. W. McCurdy, and F. Martín, Phys. Rev. Lett. **110**, 173001 (2013).
[40] F. L. Yip, C. W. McCurdy, and T. N. Rescigno, Phys. Rev. A **81**, 063419 (2010).
[41] F. L. Yip, F. Martín, C. W. McCurdy, and T. N. Rescigno, Phys. Rev. A **84**, 053417 (2011).
[42] J. M. Feagin, J. Phys. B **31**, L729 (1998).
[43] M. Walter and J. S. Briggs, Phys. Rev. Lett. **85**, 1630 (2000).
[44] A. S. Kheifets and I. Bray, Phys. Rev. A **72**, 022703 (2005).
[45] A. S. Kheifets, Phys. Rev. A **71**, 022704 (2005).
[46] W. Vanroose, F. Martín, T. N. Rescigno, and C. W. McCurdy, Science **310**, 1787 (2005).
[47] W. Vanroose, D. A. Horner, F. Martín, T. N. Rescigno, and C. W. McCurdy, Phys. Rev. A **74**, 052702 (2006).
[48] D. A. Horner, W. Vanroose, T. N. Rescigno, F. Martín, and C. W. McCurdy, Phys. Rev. Lett. **98**, 073001 (2007).
[49] L. Tao, C. W. McCurdy, and T. N. Rescigno, Phys. Rev. A **82**, 023423 (2010).
[50] D. A. Horner, S. Miyabe, T. N. Rescigno, C. W. McCurdy, F. Morales, and F. Martín, Phys. Rev. Lett. **101**, 183002 (2008).
[51] J. Colgan, M. S. Pindzola, and F. Robicheaux, Phys. Rev. Lett. **98**, 153001 (2007).
[52] T. J. Reddish, J. Colgan, P. Bolognesi, L. Avaldi, M. Gisselbrecht, M. Lavollée, M. S. Pindzola, and A. Huetz, Phys. Rev. Lett. **100**, 193001 (2008).
[53] J. Colgan, M. S. Pindzola, and F. Robicheaux, J. Phys. B **41**, 121002 (2008).
[54] X. Guan, K. Bartschat, and B. I. Schneider, Phys. Rev. A **83**, 043403 (2011).
[55] I. A. Ivanov and A. S. Kheifets, Phys. Rev. A **85**, 013406 (2012).
[56] W.-C. Jiang, L.-Y. Peng, J.-W. Geng, and Q. Gong, Phys. Rev. A **88**, 063408 (2013).
[57] D. Reedy, J. B. Williams, B. Gaire, A. Gatton, M. Weller, A. Menssen, T. Bauer, K. Henrichs, Ph. Burzynski, B. Berry, Z. L. Streeter, J. Sartor, I. Ben-Itzhak, T. Jahnke, R. Dörner, Th. Weber, and A. L. Landers, Phys. Rev. A **98**, 053430 (2018).
[58] J. E. Sansonetti and W. C. Martin, J. Phys. Chem. Ref. Data **34**, 1559 (2005).
[59] B. Gervais, E. Giglio, L. Adoui, A. Cassimi, D. Duflot, and M. E. Galassi, J. Chem. Phys. **131**, 024302 (2009).
[60] H.-J. Werner, P. J. Knowles, G. Knizia, F. R. Manby, and M. Schütz, WIREs Comput. Mol. Sci. **2**, 242 (2012).
[61] H.-J. Werner, P. J. Knowles, G. Knizia, F. R. Manby, M. Schütz *et al.*, Molpro, version 2015.1, a package of *ab initio* programs, 2015, see http://www.molpro.net.
[62] T. H. D. Jr., J. Chem. Phys. **90**, 1007 (1989).
[63] H. Lischka, T. Müller, P. G. Szalay, I. Shavitt, R. M.Pitzer, and R. Shepard, WIREs Comput. Mol. Sci. **1**, 191 (2011).
[64] H. Lischka, R. Shepard, R. M. Pitzer, I. Shavitt, M. Dallos, T. Muller, P. G. Szalay, M. Seth, G. S. Kedziora, S. Yabushita, and Z. Zhang, Phys. Chem. Chem. Phys. **3**, 664 (2001).
[65] H. Lischka, R. Shepard, I. Shavitt, R. M. Pitzer, M. Dallos, T. Müller, P. G. Szalay, F. B. Brown, R. Ahlrichs, H. J. Bm, A. Chang, D. C. Comeau, R. Gdanitz, H. Dachsel, C. Ehrhardt, M. Ernzerhof, P. Höchtl, S. Irle, G. Kedziora, T. Kovar *et al.*, Columbus, an *ab initio* electronic structure program, release 7.0, 2015.
[66] E. Wigner, Phys. Rev. **40**, 749 (1932).
[67] R. de Vivie, C. M. Marian, and S. D. Peyerimhoff, Chem. Phys. **112**, 349 (1987).
[68] R. N. Zare, Mol. Photochem. **4**, 1 (1972).
[69] H. Adaniya, B. Rudek, T. Osipov, D. J. Haxton, T. Weber, T. N. Rescigno, C. W. McCurdy, and A. Belkacem, Phys. Rev. Lett. **103**, 233201 (2009).
[70] J. Colgan and M. S. Pindzola, Phys. Rev. A **65**, 022709 (2002).
[71] S. A. Abdel-Naby, M. S. Pindzola, and J. Colgan, J. Phys. B **48**, 025204 (2015).
[72] E. Sokell, P. Bolognesi, A. Kheifets, I. Bray, S. Safgren, and L. Avaldi, Phys. Rev. A **89**, 013413 (2014).